Gaussian process models for periodicity detection

N. Durrande[1*], J. Hensman[1], M. Rattray[2], N. D. Lawrence[1]
[1] Department of Computer Science and Sheffield Institute for Translational Neuroscience, University of Sheffield, UK
[2] Faculty of Life Sciences, University of Manchester, UK

March 2013

Summary. We consider the problem of detecting the periodic part of a function given the observations of some input/output tuples (x_i, y_i), $1 \leq i \leq n$. As they are known for being powerful tools for dealing with such data, our approach is based on Gaussian process regression models which are closely related to reproducing kernel Hilbert spaces (RKHS). The latter offer a powerful framework for decomposing covariance functions as the sum of periodic and aperiodic kernels. This decomposition allows for the creation of sub-models which capture the periodic nature of the signal and its complement. To quantify the periodicity of the signal, we derive a periodicity ratio which reflects the uncertainty in the fitted sub-models. Although the method can be applied to many kernels, we give a special emphasis to the Matérn family, from the expression of the RKHS inner product to the implementation of the associated periodic kernels in a Gaussian process toolkit. The efficiency of the proposed method is finally illustrated on a biological case study where we detect periodically expressed genes.

Keywords. Harmonic analysis, RKHS, Kriging, Matérn kernels.

1 Introduction

The periodic behaviour of natural phenomena arises at many scales, from the small wavelength of electromagnetic radiations to the movements of planets. The mathematical study of natural cycles can be traced back to the XIX century with Thompson's harmonic analysis for predicting tides [Thomson, 1878] and Schuster's investigations on the periodicity of sunspots [Schuster, 1898]. Amongst the methods that have been considered for detecting

*Corresponding author: n.durrande@sheffield.ac.uk

and extracting the periodic trend, one can cite harmonic analysis [Hartley, 1949], folding methods [Stellingwerf, 1978, Leahy et al., 1983] which are mostly used in astrophysics and periodic autoregressive models [Troutman, 1979, Vecchia, 1985]. In this article, we will focus on the application of harmonic analysis in reproducing kernel Hilbert spaces (RKHS) and on the consequences for Gaussian Process (GP) modelling.

Harmonic analysis is based on the projection of a function on a basis of periodic functions. For example, a natural method for extracting the 2π-periodic trend of a function f is to decompose it in a Fourier series:

$$f(x) \to f_p(x) = a_1 \sin(x) + a_2 \cos(x) + a_3 \sin(2x) + a_4 \cos(2x) + \dots \tag{1}$$

where the coefficients a_i are given, up to a normalising constant, by the L^2 inner product between f and the elements of the basis. However, the phenomenon under study is often observed in a limited number of points, which means that the value of $f(x)$ is not known for all x but only for a small set of inputs $\{x_1, \dots, x_n\}$ called the observation points. With this limited knowledge of f, it is not possible to compute the integrals of the L^2 inner product so the coefficients a_i cannot be obtained directly.

A popular approach to overcome the fact that f is partially known is to build a mathematical model m to approximate it. A good model m has to take into account as much information as possible about f. Typically, it interpolates f for the set of observation points $m(x_i) = f(x_i)$ and its differentiability corresponds to the assumptions one can have about the regularity of f. The main body of literature tackling the issue of interpolating spatial data is scattered over three fields: (geo-)statistics [Matheron, 1963, Stein, 1999], functional analysis [Aronszajn, 1950, Berlinet and Thomas-Agnan, 2004] and machine learning [Rasmussen and Williams, 2006]. In the first case, the solution of the interpolation corresponds to the conditional expectation of a Gaussian process Z and in the second, it is the interpolator with minimal norm in a particular Hilbert space $\mathcal{H}$. As many authors pointed out (see for example Berlinet and Thomas-Agnan [2004], Scheuerer et al. [2011]), the two approaches are closely related. Both Z and $\mathcal{H}$ are based on a common object which is a positive definite function of two variables $k(.,.)$. In statistics, k corresponds to the covariance of Z and for the functional counterpart, k is the reproducing kernel of $\mathcal{H}$. From the interpolation or regularization point of view, the two approaches are equivalent since they lead to the same model m [Wahba, 1990]. Although we will focus hereafter on the RKHS framework to design periodic kernels, we will also take advantage of the powerful probabilistic interpretation offered by Gaussian processes.

A naive approach for extracting the periodic part of f given some observations would be to approximate it with a mathematical model m and to compute the Fourier coefficients of m. However, this method is not fully satisfactory since each step involves an orthogonal projection for a different norm. In other words, the construction of m and the computation of the coefficients are optimal, but not for the same criterion. As a result the periodic part obtained with this method cannot naturally be seen as a "best predictor". To overcome this issue, we propose in this article to build the Fourier series using the RKHS inner product instead of the L^2 one. To do so, we extract the sub-RKHS $\mathcal{H}_p$ of periodic functions in $\mathcal{H}$ and model the periodic part of f by its orthogonal projection onto $\mathcal{H}_p$. The prediction then inherits from the probabilistic framework associated with RKHS and the percentage of periodicity of f can elegantly be estimated.

The last part of this introduction, gives an overview of the RKHS framework and emphasises the properties of the Matérn family of kernels. In section 2, we focus on the construction of periodic kernels. Section 3 details the decomposition of GP models into periodic and aperiodic sub-model. These results allow us to introduce, in Section 4, a new criterion for measuring the periodicity of a signal. Finally, the last section illustrates the proposed approach on a biological case study where we detect, amongst the entire genome, the genes presenting a cyclic expression. This issue of detecting periodically expressed genes is the application that initially motivated the present work.

The examples and the results presented in this article have been generated with the version 0.2 of the python Gaussian process toolbox *GPy*. This toolbox, in which we have implemented the periodic kernels discussed here, can be downloaded at `http://github.com/SheffieldML/GPy`.

1.1 Approximation in Reproducing Kernel Hilbert Spaces

The aim of this section is to introduce the notion of RKHS and to derive the expression of the best predictor. We will also briefly show how to construct a RKHS from any positive definite function. For a more details, we refer the reader to Berlinet and Thomas-Agnan [2004, chap. 1] and Aronszajn [1950].

Let $\mathcal{H}$ be a Hilbert space of real valued functions defined over $D \subset \mathbb{R}$. $\mathcal{H}$ is said to be a RKHS if and only if there exist a function $k(.,.) : D \times D \to \mathbb{R}$ such that for all $x \in D$

(*i*) $k(x,.) \in \mathcal{H}$

$(ii)\ \forall f \in \mathcal{H},\ f(x) = \langle f, k(x,.)\rangle_{\mathcal{H}}$.

The function k satisfying these properties is unique and it is called the *reproducing kernel* of $\mathcal{H}$.

Recalling that a function k is said to be positive semi-definite if $\forall m \in \mathbb{N},\ \forall \mathbf{a} \in \mathbb{R}^m,\ \forall \mathbf{x} \in D^m$

$$\sum_{i=1}^{m}\sum_{j=1}^{m} a_i a_j k(x_i, x_j) \geq 0, \tag{2}$$

it can be shown that a reproducing kernel is necessarily a symmetric positive semi-definite (spd) function. Reciprocally, the Moore-Aronszajn theorem states that for all spd-function k on $D \times D$, there exist only one RKHS of functions on D with k as reproducing kernel. A common approach is then to define a RKHS by specifying its reproducing kernel. As the covariance of a random process is also a spd-function, we will use interchangeably the words kernel, covariance function and reproducing kernel.

To get an insight on the elements of the RKHS associated with a spd-function k, we first consider the space H generated by finite combinations of $k(x_i, .)$:

$$H = \left\{ \sum_{i=1}^{m} a_i k(x_i, .),\ a_i \in \mathbb{R},\ x_i \in D,\ m \in \mathbb{N} \right\}. \tag{3}$$

Obviously, we have $k(x, .) \in H$ for all $x \in D$ so (i) is satisfied. Using the property that k is a spd-function, it is straightforward to show that

$$\left\langle \sum_{i=1}^{m} a_i k(x_i, .), \sum_{j=1}^{m'} b_j k(x_j, .) \right\rangle_H = \sum_{i=1}^{m}\sum_{j=1}^{m'} a_i b_j k(x_i, x_j). \tag{4}$$

defines a valid inner product on H. One particular asset of this inner product is that $k(x, .)$ satisfies (ii). Indeed, for all $f = \sum a_i k(x_i, .) \in \mathcal{H}$ and $x \in D$ we have

$$\langle f, k(x, .)\rangle_H = \sum_{i=1}^{m} a_i \langle k(x_i, .), k(x, .)\rangle_H = \sum_{i=1}^{m} a_i k(x_i, x) = f(x). \tag{5}$$

Although the properties (i) and (ii) are fulfilled, H is not a necessarily a RKHS since it may not a Hilbert space (it is not always complete). Let $\mathcal{H}$ be the closure of H and $\langle ., . \rangle_{\mathcal{H}}$ the continuous extension of $\langle ., . \rangle_H$ onto $\mathcal{H}$. Then $\mathcal{H}$ is a Hilbert space and it can be shown that (i) and (ii) are still satisfied: $\mathcal{H}$ is the only RKHS with kernel k.

We will now focus on how to take advantage of the RKHS framework to approximate a function f that is observed in a limited number of points. Let $X = \{x_1, \ldots, x_n\} \in D^n$ be a set of points where the value $y_i = f(x_i)$ is known and $\mathbf{y}$ be the vector of y_i. For a given RKHS $\mathcal{H}$, the best interpolator m is defined as the interpolator with minimal norm:

$$m = \underset{h \in \mathcal{H}}{\operatorname{argmin}} \left(||h||_{\mathcal{H}} \;\middle|\; h(x_i) = y_i,\ i \in 1, \ldots, n \right). \tag{6}$$

It can be shown that m corresponds to the orthogonal projection of f onto the space spanned by the $k(x_i, .)$:

$$\mathcal{H}_X = \operatorname{span}\left(k(x_i, .),\ x_i \in X \right). \tag{7}$$

Let $\mathbf{k}(.)$ be the $n \times 1$ vector of functions with general term $(\mathbf{k}(.))_i = k(x_i, .)$. This vector corresponds to a basis of $\mathcal{H}_X$. The Gram matrix $\mathbf{K}$ associated to this basis has general term $\mathbf{K}_{ij} = \langle k(x_i, .), k(x_j, .) \rangle_{\mathcal{H}} = k(x_i, x_j)$. When $\mathbf{K}$ is invertible, it is straightforward to show that

$$k_X(x, y) = \mathbf{k}^T(x) \mathbf{K}^{-1} \mathbf{k}(y) \tag{8}$$

satisfies (i) and (ii). Since $\mathcal{H}_X$ is a finite dimensional space it is necessarily complete so $\mathcal{H}_X$ is a RKHS with reproducing kernel k_X. The orthogonal projection of f onto $\mathcal{H}_X$ is then:

$$m(x) = \langle k_X(x, .), f \rangle_{\mathcal{H}} = \mathbf{k}^T(x) \mathbf{K}^{-1} \langle \mathbf{k}(.), f \rangle_{\mathcal{H}} = \mathbf{k}^T(x) \mathbf{K}^{-1} \mathbf{y}. \tag{9}$$

In the geostatistical community, m is referred to as the Kriging mean. In the probabilistic framework, this expression corresponds to the conditional expectation of a centred Gaussian process Z with covariance k knowing the observations. Furthermore, GP provide naturally some prediction variance for the model:

$$\begin{aligned} m(x) &= \mathrm{E}[Z(x) | Z(x_i) = y_i] = \mathbf{k}^T(x) \mathbf{K}^{-1} \mathbf{y} \\ v(x) &= \mathrm{Var}[Z(x) | Z(x_i) = y_i] = k(x, x) - \mathbf{k}^T(x) \mathbf{K}^{-1} \mathbf{k}(x) \end{aligned} \tag{10}$$

One particular asset of Eqs. 9-10 is that the expressions of $m,\ v$ only depends on k. As a result it is not necessary to derive the expression of the inner product generated by k to obtain the best predictor and any spd-function can be used directly to build models. However, a direct proof of the positive definiteness of a function is often intractable and a widespread approach is to use well known spd-functions such as the squared-exponential (i.e. Gaussian and radial basis function) or the spline kernel. The next section recalls some results about another interesting class of spd-functions: the Matérn family.

1.2 The Matérn class of kernels

Matérn kernels k are stationary spd-functions, which means that they only depend on the distance between the points they are evaluated at: $k(x, y) = \tilde{k}(|x - y|)$. They are often introduced by the spectral density of $\tilde{k}$ [Stein, 1999]:

$$S(\omega) = \left(\frac{\Gamma(\nu)\theta^{2\nu}}{2\sigma^2\sqrt{\pi}\Gamma(\nu + 1/2)(2\nu)^\nu} \left(\frac{2\nu}{\theta^2} + \omega^2 \right)^{\nu+1/2} \right)^{-1}. \tag{11}$$

Three parameters can be identified in this equation: ν which tunes the differentiability of $\tilde{k}$, θ which corresponds to a lengthscale parameter and σ^2 that is homogeneous to a variance. Note that all these parameters are positive reals.

The actual expressions of the Matérn kernels are simple when the parameter ν is half-integer. For $\nu = 1/2,\ 3/2,\ 5/2$ we have

$$\begin{aligned} k_{1/2}(x, y) &= \sigma^2 \exp\left(-\frac{|x - y|}{\theta} \right) \\ k_{3/2}(x, y) &= \sigma^2 \left(1 + \frac{\sqrt{3}|x - y|}{\theta} \right) \exp\left(-\frac{\sqrt{3}|x - y|}{\theta} \right) \\ k_{5/2}(x, y) &= \sigma^2 \left(1 + \frac{\sqrt{5}|x - y|}{\theta} + \frac{5|x - y|^2}{3\theta^2} \right) \exp\left(-\frac{\sqrt{5}|x - y|}{\theta} \right). \end{aligned} \tag{12}$$

It can be seen that the parameters θ and σ^2 respectively correspond to a rescaling of the abscissa and ordinate axis. For $\nu = 1/2$ one can recognise the expression of the exponential kernel (i.e. the covariance of the Ornstein-Uhlenbeck process) and the limit case $\nu \to \infty$ corresponds to the squared exponential covariance function [Rasmussen and Williams, 2006].

One considerable asset of the Matérn class of kernels is to have strong connections with various fields. For example, a Gaussian process Z with Matérn covariance is an autoregressive process. As detailed in appendix A, this connection allows to use previous results from the literature to derive the expression of the inner products of the associated RKHS:

Matérn 1/2 (exponential kernel)

$$\langle g, h \rangle_{\mathcal{H}_{1/2}} = \frac{\theta}{2\sigma^2} \int_a^b \left(\frac{1}{\theta} g + g' \right) \left(\frac{1}{\theta} h + h' \right) \mathrm{d}t + \frac{1}{\sigma^2} g(a) h(a) \tag{13}$$

Matérn 3/2

$$\begin{aligned}\langle g,h\rangle_{\mathcal{H}_{3/2}} = \frac{\theta^3}{12\sqrt{3}\sigma^2}\int_a^b \left(\frac{3}{\theta^2}g + 2\frac{\sqrt{3}}{\theta}g' + g''\right)\left(\frac{3}{\theta^2}h + 2\frac{\sqrt{3}}{\theta}h' + h''\right)\mathrm{d}t \\ + \frac{1}{\sigma^2}g(a)h(a) + \frac{\theta^2}{3\sigma^2}g'(a)h'(a)\end{aligned} \tag{14}$$

Matérn 5/2

$$\begin{aligned}L_t(g) &= \sqrt{\frac{3\theta^5}{400\sqrt{5}\sigma^2}}\left(\frac{5\sqrt{5}}{\theta^3}g(t) + \frac{15}{\theta^2}g'(t) + \frac{3\sqrt{5}}{\theta}g''(t) + g'''(t)\right) \\ \langle g,h\rangle_{\mathcal{H}_{5/2}} &= \int_a^b L_t(g)L_t(h)\mathrm{d}t + \frac{9}{8\sigma^2}g(a)h(a) + \frac{9\theta^4}{200\sigma^2}g(a)''h''(a) \\ &\quad + \frac{3\theta^2}{5\sigma^2}\left(g'(a)h'(a) + \frac{1}{8}g''(a)h(a) + \frac{1}{8}g(a)h''(a)\right)\end{aligned} \tag{15}$$

Although these expressions are direct consequences of Doob [1953] and Hájek [1962] they cannot be found in the literature to the best of our knowledge.

Another field that is closely related to Matérn kernels is Sobolev spaces. As stated in Porcu and Stein [2012, Theorem 9.1] and Wendland [2005], the RKHS generated by k coincides with the Sobolev space $W_2^{\nu+1/2}$. This will be particularly useful in the next section to show that sine and cosine functions belong to the RKHS.

Scheuerer et al. [2011] point out that Sobolev spaces are intuitively more accessible than RKHS (it is often straightforward to tell if a function belongs or not to W_2^n) but RKHS offer a good framework for deriving an approximation of f based on the observations $f(x_i)$. As a consequence, Matérn RKHS are very interesting for modelling since they benefit from both assets: the Sobolev structure of $\mathcal{H}$ allows to understand the assumptions on f (for example, ν is directly linked to differentiability of f) and the RKHS properties give a compact expression for the optimal predictor.

2 Kernels of periodic subspaces

2.1 Fourier basis in RKHS

In this section, we will see how to extract the subspace of 2π-periodic functions in a RKHS $\mathcal{H}$. We will assume here that $\mathcal{H}$ has a Matérn kernel where ν is half-integer. However, the method presented here can be applied to any RKHS as long as the Gram matrix associated to a periodic basis can be computed. For a detailed list of RKHS inner products we refer the reader to [Berlinet and Thomas-Agnan, 2004, Chap. 7].

One popular basis for a space of periodic functions is the Fourier basis ($\sin(x)$, $\cos(x)$, $\sin(2x)$, $\cos(2x)$, ...). Hereafter, we consider a truncated version of this basis, ignoring the frequencies higher than q

$$\mathbf{F}(x) = (\sin(x), \cos(x), \ldots, \sin(qx), \cos(qx))^T, \tag{16}$$

and we denote by $\mathcal{H}_p$ the space spanned by this basis. The fact that $\mathcal{H}$ coincides with $W_2^{\nu+1/2}$ ensures that the elements of $\mathcal{H}$ are the functions such that

- the i^{th} derivatives ($0 \leq i \leq \nu - 1/2$) are absolutely continuous and square integrable,
- the $(\nu + 1/2)^{\text{th}}$ derivative is defined almost everywhere and is square integrable.

As a consequence, we have $\mathcal{H}_p \subset \mathcal{H}$ since all the functions of the basis are infinitely differentiable. Let $\mathbf{G}$ be the Gram matrix of $\mathbf{F}$ in $\mathcal{H}$: $\mathbf{G}_{i,j} = \langle \mathbf{F}_i, \mathbf{F}_j \rangle_{\mathcal{H}}$. Similarly to Eq. 8, it is straightforward to show that

$$k_p(x, y) = \mathbf{F}^T(x)\mathbf{G}^{-1}\mathbf{F}(y) \tag{17}$$

is the reproducing kernel of $\mathcal{H}_p$. Hereafter, we will refer to k_p as the *periodic kernel*.

The matrix $\mathbf{G}$ can be computed from the expression of the inner product given in Eqs. 13-15. In contrast to the Gram matrix of the Fourier basis in L^2, $\mathbf{G}$ is not a diagonal matrix if the length of D is a multiple of the period. One essential property for the practical use of periodic kernels is that the computation of the elements of $\mathbf{G}$ can be performed analytically. Indeed, all the elements of the basis can be written in the form $\cos(\omega x + \varphi)$. Using the notation L_x for the linear operators in the inner product integrals (see Eq. 15) we obtain:

$$L_x(\cos(\omega x + \varphi)) = \sum_i \alpha_i \cos(\omega x + \varphi)^{(i)} = \sum_i \alpha_i \omega^i \cos\left(\omega x + \varphi + \frac{i\pi}{2}\right). \tag{18}$$

The latter can be factorised in a single cosine $\rho\cos(\omega x + \phi)$ with

$$\rho = \sqrt{r_c^2 + r_s^2}, \quad \phi = \begin{cases} \arcsin(r_s/\rho) & \text{if } r_c \geq 0 \\ \arcsin(r_s/\rho) + \pi & \text{if } r_c < 0 \end{cases} \tag{19}$$

where $r_c = \sum_i \alpha_i \omega^i \cos\left(\varphi + \frac{i\pi}{2}\right)$ and $r_s = \sum_i \alpha_i \omega^i \sin\left(\varphi + \frac{i\pi}{2}\right)$.

Eventually, the computation of the inner product boils down to the integration of a product of two cosines, which can be solved by linearisation.

2.2 Tuning the period

We assumed previously a 2π-periodicity for the signal. However this period can be modified by introducing a parameter λ in the definition of the Fourier basis:

$$\mathbf{F}_\lambda(x) = \left(\sin\left(\frac{2\pi}{\lambda}x\right),\ \ldots,\ \cos\left(\frac{2\pi}{\lambda}qx\right)\right)^T. \tag{20}$$

As for the other parameters of the kernel σ^2 and θ, maximum likelihood estimation can be used to obtain a value of λ well suited to the data. This estimation of the period will be illustrated in the case study of the next section.

2.3 Application to a benchmark

We will now illustrate on a benchmark of test functions the use periodic kernels for GP modelling. Furthermore, we will compare the resulting models with COSOPT [Straume, 2004] and ARSER [Yang and Su, 2010] which are representative of the methods commonly used in biostatistics for detecting periodically expressed genes [Hughes et al., 2009, Amaral and Johnston, 2012].

COSOPT assumes the following model for the signal:

$$y(t) = \alpha + \beta t + \gamma\cos(\omega t + \varphi) + \varepsilon, \tag{21}$$

where ε corresponds to some white noise. The algorithm proceeds in two steps to determine the values of α, β, γ, ω and φ. First, a linear regression model is fitted to estimate the value of $\alpha,\ \beta$. The linear trend is then subtracted from the signal and the remaining parameters are fitted by minimizing the mean square error.

The underlying model is more sophisticated for ARSER since it accounts for various frequencies:

$$y(t) = \alpha + \beta t + \sum_i \gamma_i\cos(\omega_i t + \varphi_i) + \varepsilon. \tag{22}$$

The number of cosine terms and their frequencies ω_i are obtained by detecting the peaks of the spectrum via the fast Fourier transform. In practice, this number is typically around 1-5. As previously the linear trend is initially subtracted to the data and an additional smoothing is performed to limit high frequencies due to noise. Although this model is more flexible, it has two drawbacks: the input points are assumed to be regularly spaced and the resulting model is not necessarily periodic.

In addition, we introduce the following Gaussian process model:

$$Y(t) = \alpha + \beta t + Y_p(t) + \varepsilon. \tag{23}$$

where Y_p has periodic kernel k_p. Here, α and β should be interpreted as random variables with Gaussian distribution $\mathcal{N}(0,1)$. The best predictor associated with this model given by Eq. 9) where $k(x,y) = 1 + xy + \sigma_p^2 k_p(x,y) + \tau^2\delta(x,y)$. The parameters σ_p^2, θ, λ and τ^2 are obtained by maximising the likelihood of the observations. This is equivalent to minimizing -2 times the log-likelihood:

$$\mathcal{L} = n\log(2\pi) + \log|\mathbf{K}| + \mathbf{Y}^T\mathbf{K}^{-1}\mathbf{Y} \tag{24}$$

which depends on all the parameters of the kernel through the matrix $\mathbf{K}$. The number of frequencies in the Fourier basis is set to $q = 20$. The best predictor associated with this model given by Eq. 9 where $k(x,y) = 1 + xy + k_p(x,y) + \tau^2\delta_{x,y}$. Although this information is readily available, we will not use in this benchmark the prediction variance provided by the GP models.

COSOPT and ARSER also include additional features for measuring the periodicity of a signal in term of p-value or false discovery rate. The probabilistic framework of Gaussian processes could be used to derive such statistics for the proposed model but these developments fall out of the scope of the present article.

The prediction of these models are compared on a benchmark of 1-periodic test functions defined over $[0,3]$: $\cos(2\pi t)$, $\text{sumcos}(t) = 1/2(\cos(2\pi t) + \cos(4\pi t))$, $\text{square}(t)$, $\text{triangle}(t)$, $\text{diag}(t)$ and $\text{noise}(t)$ which are represented in Figure 1. A training set of 50 equally spaced test points is used for learning these functions and a $\mathcal{N}(0, 0.1)$ observation noise is added to each observation, except for noise where the perturbations are $\mathcal{N}(0,1)$. As the test functions do not include any linear trend, the value of β is fixed to zero for all models.

The models fitted with COSOPT, ARSER and the periodic GP can be compared in Figure 2. To asses the overall precision, we repeat the fitting procedure 50 times with different values of the observation noise. The root mean square error (RMSE) is computed based on a 500-point test set spanning $[0,3]$. A summary of the obtained result is given in Table 1.

Many remarks can be formulated based on the observation of Figure 2 and Table 1. First, COSOPT gives a good fit for the cosine function, but also for the triangular test function. This can be explained by the overall cosine shape of the latter. The noise filtering can be

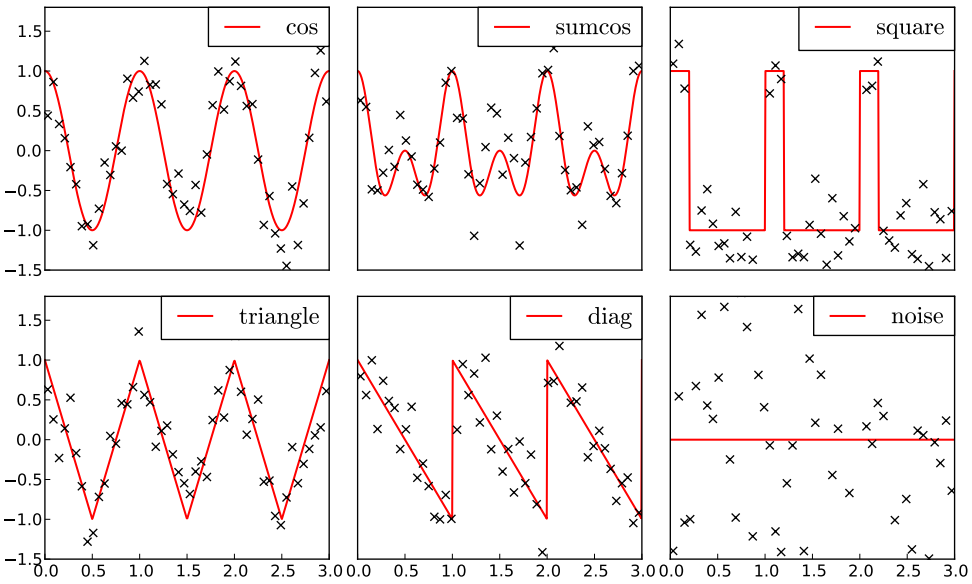

Figure 1: Test functions considered in the benchmark. The crosses indicate the observed values after adding the random noise.

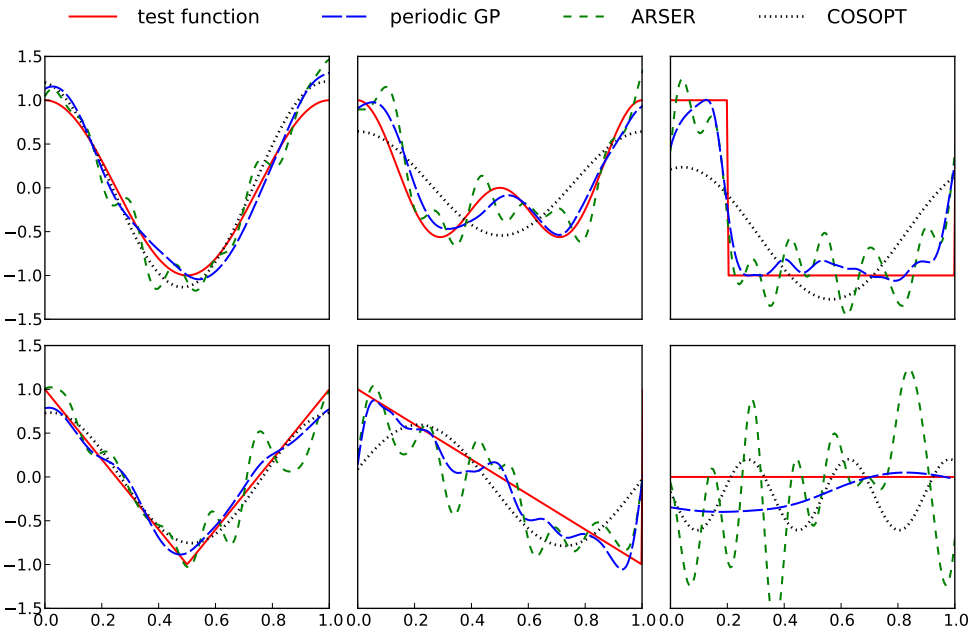

Figure 2: Plots of the test functions with associated fitted models. For an improved visibility, the plotting region is limited to one period. The periodic GP model is based on a periodic Matérn kernel with regularity $\nu = 3/2$.

test function	COSOPT	ARSER	GP $\nu = 1/2$	GP $\nu = 3/2$	GP $\nu = 5/2$
cos	***0.09*** (0.03)	0.23 (0.03)	0.16 (0.03)	**0.11** (0.03)	**0.10** (0.03)
sumcos	0.36 (0.01)	0.24 (0.08)	0.19 (0.09)	**0.14** (0.04)	***0.13*** (0.04)
square	0.60 (0.01)	0.37 (0.03)	***0.31*** (0.05)	**0.32** (0.04)	**0.32** (0.03)
triangle	***0.11*** (0.02)	0.23 (0.03)	0.15 (0.03)	**0.12** (0.03)	**0.12** (0.03)
diag	0.36 (0.01)	0.33 (0.04)	***0.26*** (0.04)	***0.26*** (0.03)	***0.26*** (0.03)
noise	**0.40** (0.06)	0.73 (0.11)	**0.44** (0.20)	**0.39** (0.19)	***0.37*** (0.21)
mean	0.32	0.36	0.25	0.22	0.22

Table 1: Mean value (and standard deviation) of RMSE for each test function and model. The best fit is indicated in italic. The models within one standard deviation from the best result are indicated in bold.

judged satisfactory for this model but, as expected, the model fails to approximate non-sinusoidal patterns such as square and sumcos. The wider range of frequencies allowed in ARSER makes it capable of approximating these more complicated patterns. The drawback for this model is its sensitivity to noise. Indeed high frequencies oscillations corresponding to noise overfitting can be observed on ARSER models. Although some functions in the test set are typically difficult to approximate with Gaussian process models due the presence of discontinuity, the models based on periodic kernels perform remarkably well on this benchmark. On the one hand, the large number of frequencies considered in the truncated Fourier basis allows a good fit of non-sinusoidal patterns. On the other, the embedding of this basis into a Matérn RKHS naturally imposes a penalty on the high frequencies which results in a good filtering of the noise.

Note that the results obtained for the periodic GP models are not specific to the class of periodic kernel introduced in this article. Usual periodic kernels such as $k(x, y) = \exp\left(-(\sin(|x - y|)^2\right)$ (see Rasmussen and Williams [2006] for more details) would probably lead to similar results. We will detail in the next section one particular asset of the proposed kernels in term of decomposition of the signal.

3 Decomposition of models

3.1 Decomposition of kernels

The difference of two kernels is generally not a valid covariance function. However the construction of k_p ensures that, in this particular case, $k_a = k - k_p$ corresponds to a kernel.

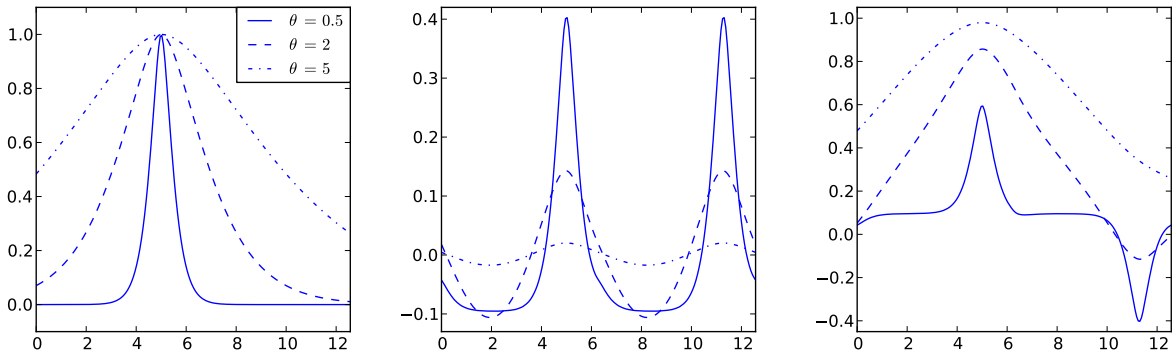

(a) Matérn kernel k. (b) periodic sub-kernel k_p. (c) aperiodic sub-kernel k_a.

Figure 3: Examples of decompositions of a Matérn 3/2 kernel as a sum of a periodic and aperiodic sub-kernels. The three graphs on each plot correspond to a different value of the lengthscale parameter θ. For this example the input space is $D = [0, 4\pi]$, the cut-off frequency is $q = 20$ and one of the variables of the kernels is arbitrarily fixed to 5.

This is straightforward to see using the RKHS framework since k_a is the reproducing kernel of the orthogonal complement of $\mathcal{H}_p$ in $\mathcal{H}$ [Berlinet and Thomas-Agnan, 2004]. As this space is orthogonal to the (truncated) Fourier basis, it will be referred to as the subspace of *aperiodic* functions (hence the subscript a). From the probabilistic point of view, this decomposition corresponds to the decomposition of Z as a sum of two independent Gaussian processes, with covariance functions k_p and k_a. This can be summarized as follow:

$$k = k_p + k_a, \qquad \mathcal{H} = \mathcal{H}_p \overset{\perp}{+} \mathcal{H}_a, \qquad Z = Z_p \overset{\perp\!\!\!\perp}{+} Z_a. \tag{25}$$

An illustration of the decomposition of Matérn 3/2 kernels can be found in Figure 3.

3.2 Periodic and aperiodic sub-models

The expressions of Eq. 25 allow decomposition of the best predictor as a sum of two sub-models m_p and m_p:

$$\begin{aligned} m(t) &= \mathrm{E}[Z_p(t) + Z_a(t) | Z(t_i) = y_i] \\ &= \mathrm{E}[Z_p(t) | Z(t_i) = y_i] + \mathrm{E}[Z_a(t) | Z(t_i) = y_i] \\ &= \mathbf{k}_p(t)^T \mathbf{K}^{-1} \mathbf{y} + \mathbf{k}_a(t)^T \mathbf{K}^{-1} \mathbf{y}. \end{aligned} \tag{26}$$

Similarly, prediction variances are associated to the sub-models

$$\begin{aligned} v_p(t) &= \mathrm{Var}[Z_p(t) | Z(t_i) = y_i] = k_p(t,t) - \mathbf{k}_p(t)^T \mathbf{K}^{-1} \mathbf{k}_p(t) \\ v_a(t) &= \mathrm{Var}[Z_a(t) | Z(t_i) = y_i] = k_a(t,t) - \mathbf{k}_a(t)^T \mathbf{K}^{-1} \mathbf{k}_a(t). \end{aligned} \tag{27}$$

However, contrarily to Eq. 26, we have $v(t) \neq v_p(t) + v_a(t)$ since Y_p and Y_a are not independent knowing the observations. For a detailed discussion on the decomposition of models based on a sum of kernels see Durrande et al. [2012].

The sub-models can be interpreted as usual GP models with correlated noise. For example, m_p is the best predictor based on kernel k_p with an observational noise given by $\mathbf{K}_a$. For the RKHS framework, m_p and m_a correspond to the solution of a regularization problem and they respectively belong to $\mathcal{H}_p$ and $\mathcal{H}_a$.

We now illustrate this model decomposition on the Mauna Loa Observatory dataset [Keeling et al., 2009] which is frequently used in modelling [Rasmussen and Williams, 2006, Wilson and Adams, 2013]. This dataset contains the monthly average of CO_2 concentration in the atmosphere since 1958, expressed in micromol of CO_2 per mol of dry air. Hereafter we will focus on the first six years of the time series, using the initial 48 time points as training data and predicting for the following 24 months. For this dataset we will assume that the one-year period is known.

We first consider a GP regression model based on a regular Matérn 3/2 kernel, with maximum likelihood estimation of σ^2, θ and τ^2. Figure 4 represents the decomposition of the model as detailed in Eqs. 26-27. It can be seen that the periodic sub-model successfully extracts the periodic component. Although this model gives very accurate predictions in the training region it drastically fails to forecast the behaviour of the signal after the last observation. We will now see how to improve this result using the sub-kernels.

3.3 Parametrisation of the kernel

A Matérn kernel k initially depends on three parameters: the regularity ν, its variance σ^2 and its lengthscale θ. However, the decomposition $k = k_p + k_a$ allows us to set the values of those parameters separately for each sub-kernel in order to increase the flexibility of the model. The new set of parameters of k is then $(\nu_p,\ \sigma_p^2,\ \theta_p,\ \nu_a,\ \sigma_a^2,\ \theta_a)$, to which λ may be added if the period is unknown.

After reparametrisation, k belongs to a larger family of kernels that encapsulates the Matérn one. Furthermore, if $\nu_p = \nu_a$, and $\sigma_p^2,\ \sigma_a^2 \neq 0$ the RKHS generated by k and the one associated with a Matérn kernel with equal regularity correspond to the same space, but endowed with a different norm.

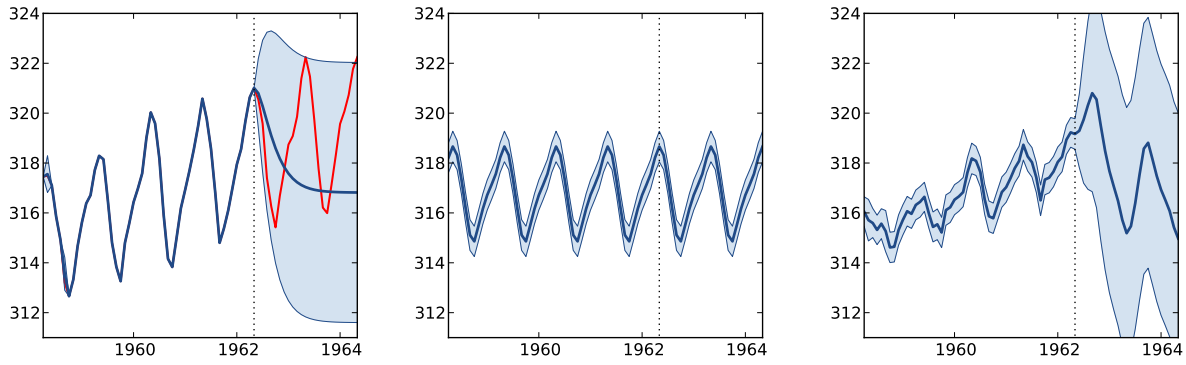

(a) global model m. (b) periodic sub-model m_p. (c) aperiodic sub-model m_a.

Figure 4: Decomposition of a model based on the Mauna Loa Observatory dataset. The model is trained on the 48 data-points contained in the left part of the graph. The kernel is Matérn 3/2, and the cut-off parameter of the Fourier basis is set to $q = 20$. The shaded area corresponds to 95% confidence intervals and the test function is represented in red. The small increase of the confidence interval width in the left of panel a is due to missing data, which is naturally supported by GP models.

The graphs presented in Figure 5 show the obtained model after estimating $(\sigma_p^2,\ \theta_p,\ \sigma_a^2,\ \theta_a)$, the regularities $(\nu_p,\ \nu_a)$ being fixed to 3/2. In this example, adding two parameters drastically improves the fit of the test function outside the observation region. The global behaviour of the phenomenon is successfully captured by the model which is capable of reproducing both the small scale patterns (oscillations) and the large scale trend. One limitation here is that the regularity parameter of the periodic and aperiodic sub-models is assumed to be the same whereas observation of data suggests a smaller differentiability order for the periodic part.

4 Measuring the periodicity

The decomposition of the model into a sum of sub-models can be used for estimating a ratio of periodicity of the signal. In sensitivity analysis, a common approach for measuring the effect of a set of variables $(x_1, \ldots, x_n)$ on the output of a multivariate function $f(x_1, \ldots, x_n)$ is to introduce a random vector $\mathbf{X} = (X_1, \ldots, X_n)$ with values in the input space of f and to define the variance explained by one subset of variables $\mathbf{x}_I = (x_{I_1}, \ldots, x_{I_m})$ as $V_I = \mathrm{Var}\left(\mathrm{E}\left(f(\mathbf{X})|\mathbf{X}_I\right)\right)$ [Oakley and O'Hagan, 2004]. Furthermore, the probabilistic features of the GP model can be taken into account by computing the indices based on random paths of the conditional GP [Marrel et al., 2009].

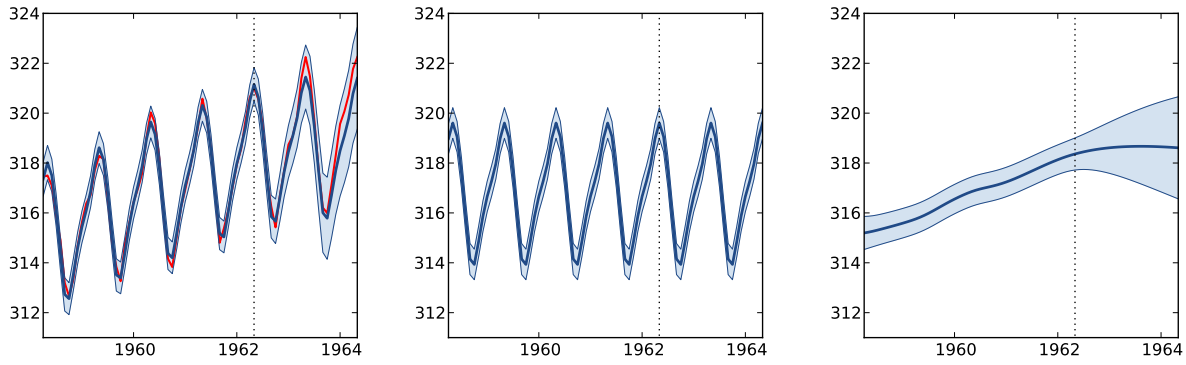

(a) global model m. (b) periodic sub-model m_p. (c) aperiodic sub-model m_a.

Figure 5: Model and sub-models after parametrisation of the kernel by $(\sigma_p^2,\ \theta_p,\ \sigma_a^2,\ \theta_a)$. The test points and the other settings are the same as in Figure 4.

We now apply these two principles to define a periodicity ratio based on the sub-models. Let T be a random variable defined over the input space and Z_p, Z_a be the periodic and aperiodic components of the conditional GP Z knowing it interpolates the data-points. Z_p and Z_a are normally distributed with respective mean and variance $(m_p,\ v_p)$, $(m_a,\ v_a)$ and their covariance is given by $\mathrm{Cov}(Z_p(t), Z_a(t')) = -\mathbf{k}_p(t)^T\mathbf{K}^{-1}\mathbf{k}_a(t')$. To quantify the periodicity of the signal we introduce the following periodicity ratio:

$$R = \frac{\mathrm{Var}_T[Z_p(T)]}{\mathrm{Var}_T[Z_p(T) + Z_a(T)]}. \tag{28}$$

Note that R does not correspond to the percentage of periodicity of the signal in a rigorous way since the dependence between Z_p and Z_a implies $\mathrm{Var}_T[Z(T)] \neq \mathrm{Var}_T[Z_p(T)] + \mathrm{Var}_T[Z_a(T)]$.

5 Application to gene expression studies

The 24 hour cycle of days can be observed in the oscillations of biological mechanisms at many scales. This phenomenon, called circadian rhythm, can for example be seen at a microscopic level on gene expressions. The cellular mechanism ensuring this periodic behaviour is called the circadian clock. For *Arabidopsis*, which is a widely used organism in plant biology and genetics, the study of the circadian clock at a gene level shows an auto-regulatory system involving several genes [Ding et al., 2007]. As advocated in Edwards et al. [2006], it is believed that the genes involved in the oscillatory mechanism have a cyclic expression so the detection of periodically expressed genes is of great interest for

completing current models. As stated in the introduction, this application is the one that motivated the work presented in this article.

The mechanism allowing genes to interfere in the functioning of the cell can be summarised as follows: DNA is first duplicated into messenger RNA, and this RNA is then used for protein synthesis. To quantify the expression of a specific gene it is thus possible to measure the concentration of RNA molecules associated with this gene. Microarray analysis and RNA-sequencing are two examples of methods that take advantage of this principle.

The dataset we consider here has been initially studied by Edwards et al. [2006][1]. It corresponds to gene expression for nine day old *arabidopsis* seedlings. After eight days under a 12h-light/12h-dark cycles, the seedlings are transferred into constant light. A microarray analysis is performed every four hours, from 26 to 74 hours after the last dark-light transition, to monitor the expression of 22810 genes. Edwards et al. [2006] use COSOPT [Straume, 2004] for detecting periodicity genes and identify a subset of 3504 periodically expressed genes, with an estimated a period between 20 and 28 hours.

We now apply to this dataset the method described in the previous sections. The kernel we consider is a sum of a periodic and aperiodic Matérn 3/2 kernel plus a delta function to reflect observation noise:

$$k(t,t') = \sigma_p^2 k_p(t,t') + \sigma_a^2 k_a(t,t') + \tau^2 \delta(t,t'). \tag{29}$$

Although the cycle of the circadian clock is known to be around 24 hours, circadian rhythms often depart from this figure (indeed circadian is Latin for *around a day*) so we introduce a parameter λ as in Sec. 2.2 to estimate the actual period. The final parametrisation of k is based on six variables: $(\sigma_p^2, \theta_p, \sigma_a^2, \theta_a, \tau^2, \lambda)$. For each gene, the values of these parameters are estimated using maximum likelihood. The optimization is based on the standard options of the GPy toolkit with the following boundary limits for the parameters: $\sigma_p,\ \sigma_a \geq 0$; $\theta_p,\ \theta_a \in [10,\ 60]$; $\tau^2 \in [10^{-5}, 0.75]$ and $\lambda \in [20,\ 28]$. Furthermore 50 random restarts are performed for each optimization to limit the effects of local minimums.

Eventually, the periodicity of each model is assessed with the ratio R given by Eq. 28. As this ratio is a random variable, we approximate the expectation of R with the mean value of 1000 realisations. To obtain results comparable with the original paper on this

[1]The original dataset is available online at `http://millar.bio.ed.ac.uk/data.htm`.

# of genes	$\mathcal{P}_{GP}$	$\overline{\mathcal{P}_{GP}}$
$\mathcal{P}_{COSOPT}$	2127	1377
$\overline{\mathcal{P}_{COSOPT}}$	1377	17929

Table 2: Confusion table associated to the predictions by COSOPT and the proposed GP approach.

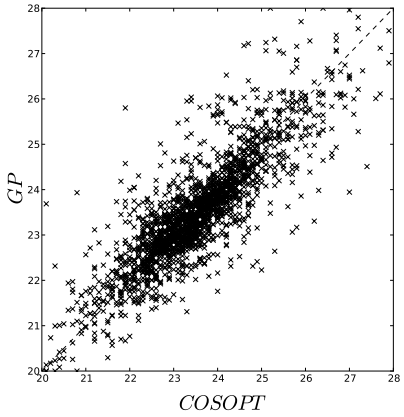

Figure 6: Estimated periods for the genes in $\mathcal{P}_{GP} \cap \mathcal{P}_{COSOPT}$. The coefficient of determination of $x \to x$ (dashed line) is 0.69.

dataset, we label as periodic the set of 3504 genes with the highest periodicity ratio. The cut-off periodicity ratio associated with this quantile is 0.77.

Let $\mathcal{P}_{COSOPT}$ and $\mathcal{P}_{GP}$ be the sets of selected periodic genes respectively by Edwards et al. [2006] and the method presented here. The overlap between the two sets is summarised in Table 2 where $\overline{\mathcal{S}}$ denotes the complement of a subset $\mathcal{S}$. Although the results cannot be compare to any ground truth, the methods seem coherent since 88% of the genes share the same label. Furthermore the estimated value of the period λ is consistent for the genes labelled as periodic by the two methods, as seen in Figure 6.

One interesting comparison between the two methods is to examine the genes that are classified differently. The available data from Edwards et al. [2006] allows focusing on the worst classification mistakes made by one method according to the other. This is illustrated in Figure 7 which shows the behaviour of the most periodically expressed genes in $\overline{\mathcal{P}_{GP}}$ according to COSOPT and, conversely, the genes in $\overline{\mathcal{P}_{COSOPT}}$ with the highest periodicity ratio R. Although it is undeniable that the genes selected only by COSOPT (panel a) present some periodic component, they also show a strong non-periodic part, corresponding either to noise or trend. For these genes, the value of the periodicity ratio is: 0.74 (0.10), 0.74 (0.15), 0.63 (0.11), 0.67 (0.05) (means and standard deviations, clockwise from top left) which is close to the classification boundary. On the other hand, the models suggested only by the GP approach show a strong periodic signal (we have for all genes

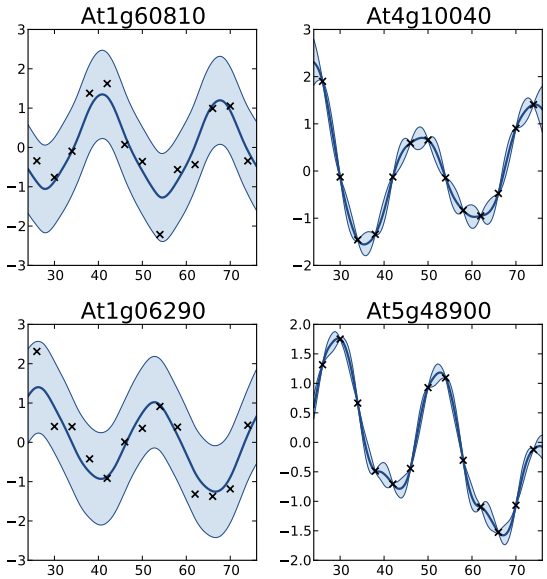

(a) Genes labelled as periodic only by COSOPT.

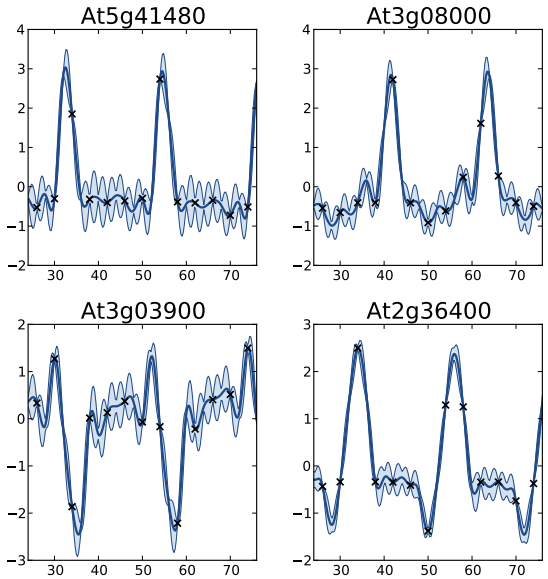

(b) Genes labelled as periodic only by the GP approach.

Figure 7: Examples of genes with different labels. The selected genes correspond to the four genes with the highest periodic part according to the method that label the gene as periodic. The titles of the graphs correspond to the name of the genes (AGI convention).

$R = 1.01$ (0.01)) with sharp spikes. Another interesting fact of panel b is that there is at least one observation associated with each spike which suggests that the behaviour of the model should not be interpreted as overfitting.

This few elements of comparison on a real life case study show some very promising results, both for the capability of the proposed method to handle large datasets and for the quality of the results. Furthermore we believe that the spike shape of the newly discovered genes may be of particular interest for understanding the mechanism of the circadian clock. The full results, as well as the original dataset can be found in the supplementary materials.

6 Conclusion

The main purpose of this article is to introduce a new approach for estimating and extracting the periodic part of a function f given some observations $f(x_i) = y_i$. As often, the proposed method corresponds to the orthogonal projection onto a basis of periodic functions. The originality here is to perform this projection in some RKHS where the partial knowledge given by the observations can be dealt with elegantly. Previous theoretical results from the mid-1900s allowed us to derive the expressions of the inner product of RKHS based on Matérn kernels. Given these results, it was then possible to define a periodic kernel k_p and to decompose k as a sum of sub-kernels $k = k_p + k_a$.

We illustrated three fundamental feature of the proposed kernels for GP modelling. First, as we have seen on the benchmark examples, they allow to approximate non-sinusoidal patterns while retaining appropriate filtering of the noise. Second, they provide a natural decomposition of the GP model as a sum of periodic and aperiodic sub-models. Third, they can be reparametrised to define a wider family of kernel which is of particular interest for decoupling the assumptions on the behaviour of the periodic and aperiodic part of the signal. This approach has proved to increase considerably the prediction ability of the model on the Mauna Loa Observatory dataset.

The probabilistic interpretation of the decomposition in sub-models is of great importance when it comes to define a criterion that quantifies the periodicity of f while taking into account the uncertainty about it. This goal was achieved by applying methods commonly used in GP based sensitivity analysis to define a periodicity ratio.

Although the proposed method can be applied to any time series data, this work has originally been motivated by the detection of periodically expressed genes. In practice

listing such genes is a key step for a better understanding of the circadian clock mechanism at a microscopic level. The effectiveness of the method is illustrated on such data in the last section. The results we obtained are consistent with the literature but they also feature some new genes with a strong periodic component. This suggest that the approach described here is not only theoretically elegant but also efficient in practice.

As a final remark, we would like to stress that the proposed method is fully compatible with all the features of Gaussian processes, from the combination of one-dimensional periodic kernels to obtain periodic kernels in higher dimension to the use of global optimisation routines such as EGO.

AKNOWLEDGEMENT

The authors gratefully acknowledge the support from the BioPreDynProject (Knowledge Based Bio-Economy EU grant Ref 289434) and the BBSRC grant BB/1004769/1.

SUPPLEMENTARY MATERIAL

The following datasets are made available under the Public Domain Dedication and License v1.0 whose full text can be found at: `http://www.opendatacommons.org/licenses/pddl`.

Case study dataset: Original dataset with the gene expressions for each gene at each time point. (csv file)

Case study results: File regrouping the available results from Edwards et al. [2006] and the one obtained in the application section. For both methods, the file gives the value of the criterion and the estimated period. (csv file)

APPENDIX

A Norms in Matérn RKHS

A.1 Autoregressive processes and RKHS norms

A process is said to be autoregressive (AR) if the spectral density of the kernel

$$S(\omega) = \frac{1}{2\pi} \int_{\mathbb{R}} k(t) e^{-i\omega t} \mathrm{d}\omega \tag{30}$$

can be written as a function of the form

$$S(\omega) = \frac{1}{\left|\sum_{k=0}^{m} \alpha_k (i\omega)^k\right|^2} \tag{31}$$

where the polynomial $\sum_{k=0}^{m} \alpha_k x^k$ is real with no zeros in the right half of the complex plan Doob [1953]. Hereafter we assume that $m \geq 1$ and that $\alpha_0, \alpha_m \neq 0$.

For such kernels, the inner product of the associated RKHS $\mathcal{H}$ is given by Hájek [1962], Kailath [1971], Parzen [1961]

$$\langle h, g \rangle_{\mathcal{H}} = \int_a^b (L_t h)(L_t g) \mathrm{d}t + 2 \sum_{\substack{0 \leq j,k \leq m-1 \\ j+k \text{ even}}} d_{j,k} h^{(j)}(a) g^{(k)}(a) \tag{32}$$

$$\text{where } L_t h = \sum_{k=0}^{m} \alpha_k h^{(k)}(t) \text{ and } d_{j,k} = \sum_{i=\max(0, j+k+1-n)}^{\min(j,k)} (-1)^{(j-i)} \alpha_i \alpha_{j+k+1-i}.$$

We show in the next section that the Matérn kernels correspond to autoregressive kernels and, for the usual values of ν, we derive the norm of the associated RKHS.

A.2 Application to Matérn kernels

Following the pattern exposed in Doob [1953, p. 542], the spectral density of a Matérn kernel (Eq. 11) can be written as the density of an AR process when $\nu + 1/2$ is an integer. Indeed, the roots of the polynomial $\frac{2\nu}{\theta^2} + \omega^2$ are conjugate pairs so it can be expressed as the squared module of a complex number

$$\frac{2\nu}{\theta^2} + \omega^2 = \left(\omega + \frac{i\sqrt{2\nu}}{\theta}\right)\left(\omega - \frac{i\sqrt{2\nu}}{\theta}\right) = \left|\omega + \frac{i\sqrt{2\nu}}{\theta}\right|^2. \tag{33}$$

Multiplying by i and taking the conjugate of the quantity inside the module, we finally obtain a polynomial in $i\omega$ with all roots in the left half of the complex plan:

$$\frac{2\nu}{\theta^2} + \omega^2 = \left|i\omega + \frac{\sqrt{2\nu}}{\theta}\right|^2 \Rightarrow \left(\frac{2\nu}{\theta^2} + \omega^2\right)^{(\nu+1/2)} = \left|\left(\frac{\sqrt{2\nu}}{\theta} + i\omega\right)^{(\nu+1/2)}\right|^2. \tag{34}$$

Plugging this expression into Eq. 11, we obtain the desired expression of S_ν:

$$S_\nu(\omega) = \frac{1}{\left|\sqrt{\frac{\Gamma(\nu)\theta^{2\nu}}{2\sigma^2\sqrt{\pi}\Gamma(\nu+1/2)(2\nu)^\nu}}\left(\frac{\sqrt{2\nu}}{\theta} + i\omega\right)^{(\nu+1/2)}\right|^2}. \tag{35}$$

Using $\Gamma(\nu) = \frac{(2\nu-1)!\sqrt{\pi}}{2^{2\nu-1}(\nu-1/2)!}$, one can derive the following expression of the coefficients α_k:

$$\alpha_k = \sqrt{\frac{(2\nu-1)!\nu^\nu}{\sigma^2(\nu-1/2)!^2 2^\nu}} \mathcal{C}^k_{\nu+1/2}\left(\frac{\theta}{\sqrt{2\nu}}\right)^{k-1/2}. \tag{36}$$

Theses values of α_k can be plugged into Eq. 32 to obtain the expression of the RKHS inner product. The results for $\nu \in \{1/2,\ 3/2,\ 5/2\}$ is given by Eqs. 13-15 in the main body of the article.

References

I. Amaral and I. Johnston. Circadian expression of clock and putative clock-controlled genes in skeletal muscle of the zebrafish. *American Journal of Physiology-Regulatory, Integrative and Comparative Physiology*, 302(1):R193–R206, 2012.

N. Aronszajn. Theory of Reproducing Kernels. *Transactions of the American Mathematical Society*, 68(3):337–404, 1950.

A. Berlinet and C. Thomas-Agnan. *Reproducing kernel Hilbert spaces in probability and statistics*. Springer, 2004.

Z. Ding, M. R. Doyle, R. M. Amasino, and S. J. Davis. A complex genetic interaction between Arabidopsis thaliana TOC1 and CCA1/LHY in driving the circadian clock and in output regulation. *Genetics*, 176(3):1501–1510, 2007.

J. L. Doob. *Stochastic processes*, volume 101. Wiley & Sons, 1953.

N. Durrande, D. Ginsbourger, and O. Roustant. Additive covariance kernels for high-dimensional Gaussian process modeling. *Annales de la faculté des Sciences de Toulouse*, XXI:481 – 499, 2012.

K. D. Edwards, P. E. Anderson, A. Hall, N. S. Salathia, J. C. W. Locke, J. R. Lynn, M. Straume, J. Q. Smith, and A. J. Millar. FLOWERING LOCUS C mediates natural variation in the high-temperature response of the Arabidopsis circadian clock. *The Plant Cell Online*, 18(3):639–650, 2006.

J. Hájek. On linear statistical problems in stochastic processes. *Czechoslovak Math. J*, 12 (87):404–444, 1962.

H. O. Hartley. Tests of significance in harmonic analysis. *Biometrika*, 36(1):194–201, 1949.

M. Hughes, L. DiTacchio, K. Hayes, C. Vollmers, S. Pulivarthy, J. Baggs, S. Panda, and J. Hogenesch. Harmonics of circadian gene transcription in mammals. *PLoS genetics*, 5 (4):e1000442, 2009.

T. Kailath. RKHS approach to detection and estimation problems–I: Deterministic signals in Gaussian noise. *IEEE Transactions on Information Theory*, 17(5):530–549, 1971.

C. D. Keeling, T. P. Whorf, A. F. Bollenbacher, and J. S. Walker. Atmospheric carbon dioxide record from Mauna Loa. Technical report, Carbon Dioxide Information Analysis Center, Oak Ridge National Laboratory, U.S. Department of Energy, 2009.

D. A. Leahy, W. Darbro, R. F. Elsner, M. C. Weisskopf, S. Kahn, P. G. Sutherland, and J. E. Grindlay. On searches for pulsed emission with application to four globular cluster X-ray sources-NGC 1851, 6441, 6624, and 6712. *The Astrophysical Journal*, 266:160–170, 1983.

A. Marrel, B. Iooss, B. Laurent, and O. Roustant. Calculations of sobol indices for the gaussian process metamodel. *Reliability Engineering & System Safety*, 94(3):742–751, 2009.

G. Matheron. Principles of geostatistics. *Economic geology*, 58(8):1246–1266, 1963.

J. E. Oakley and A. O'Hagan. Probabilistic sensitivity analysis of complex models: a Bayesian approach. *Journal of the Royal Statistical Society: Series B (Statistical Methodology)*, 66(3):751–769, 2004.

E. Parzen. An approach to time series analysis. *The Annals of Mathematical Statistics*, pages 951–989, 1961.

E. Porcu and M. L. Stein. *On Some Local, Global and Regularity Behaviour of Some Classes of Covariance Functions*, pages 221–238. Springer, 2012.

C. E. Rasmussen and C. Williams. *Gaussian Processes for Machine Learning*. MIT Press, 2006.

M. Scheuerer, R. Schaback, and M. Schlather. Interpolation of Spatial Data - A Stochastic or a Deterministic Problem? Technical report, Universität Göttingen, 2011.

A. Schuster. On the investigation of hidden periodicities with application to a supposed 26 day period of meteorological phenomena. *Terrestrial Magnetism*, 3(1):13–41, 1898.

M. L. Stein. *Interpolation of Spatial Data: some theory for kriging*. Springer Verlag, 1999.

R. F. Stellingwerf. Period determination using phase dispersion minimization. *Astrophysical Journal*, 224:953–960, 1978.

M. Straume. DNA microarray time series analysis: automated statistical assessment of circadian rhythms in gene expression patterning. *Methods in enzymology*, 383:149, 2004.

W. Thomson. Harmonic analyzer. *Proceedings of the Royal Society of London*, 27(185-189): 371–373, 1878.

B. M. Troutman. Some results in periodic autoregression. *Biometrika*, 66(2):219–228, 1979.

A. V. Vecchia. Maximum likelihood estimation for periodic autoregressive moving average models. *Technometrics*, 27(4):375–384, 1985.

G. Wahba. *Spline models for observational data*, volume 59. Society for Industrial Mathematics, 1990.

H. Wendland. *Scattered data approximation*, volume 17. Cambridge University Press, 2005.

A. G. Wilson and R. P. Adams. Gaussian Process Covariance Kernels for Pattern Discovery and Extrapolation. *arXiv preprint arXiv:1302.4245*, 2013.

R. Yang and Z. Su. Analyzing circadian expression data by harmonic regression based on autoregressive spectral estimation. *Bioinformatics*, 26(12):i168–i174, 2010.